Diyala Journal of Engineering Sciences

Journal homepage: https://djes.info/index.php/djes

ISSN: 1999-8716 (Print); 2616-6909 (Online)

# Evaluation of Biochar Derived from Partial Pyrolysis of Chara Algae for Adsorption of Lead and Copper from Aqueous Solutions

Saja A. Ismael, Salah N. Farhan *

Department of Chemical Engineering, University of Diyala, 32001 Diyala, Iraq

**ARTICLE INFO**

***Article history:***
Received March 12, 2025
Revised June 16, 2025
Accepted June 29, 2025
Available online September 01,2025

***Keywords:***
Biosorption
Heavy metals
Remediation,
Algae
Biochar

**ABSTRACT**

This study aimed to evaluate the efficiency of biochar (BC) produced from Chara algae via semi-anaerobic pyrolysis as an adsorbent for removing lead ($Pb^{2+}$) and copper ($Cu^{2+}$) ions from aqueous solutions in a batch system. The preparatory process involved washing the algal biomass with tap water and deionized water, followed by a two-stage drying process: solar drying (48 h) and then thermal drying (75°C, 24 h). Dried sample was then ground into fine particles (250–400 µm) and subjected to a semi-anaerobic heat treatment at temperatures between 400 and 600°C for 50 min to adjust the physicochemical properties of the biochar. The adsorption performance was studied under a range of operating conditions, including a range of pH (2–6), contact time (10–150 min), initial heavy metal ion concentrations (20–100 mg/L), temperatures ranging from 25 to 80°C, and various adsorbent concentrations (0.1–3 g/L). The adsorbent was characterized using advanced analytical techniques. Fourier transform infrared spectroscopy (FTIR) was used to identify the functional groups active in adsorption, scanning electron microscopy (SEM) to analyze the surface structure, and energy-dispersive X-ray spectroscopy (EDS) to determine the elemental composition and confirm metal adsorption. Under best conditions (pH 6, dosage 1.0 g/L), the maximum adsorption capacities recorded were 322 mg/g for $Pb^{2+}$ and 196 mg/g for $Cu^{2+}$. The dynamic adsorption studies further confirmed the removing heavy metals from aqueous media, indicating its promise for scalable water treatment. applications.

## 1. Introduction

The problems associated with human health and the aquatic environment due to heavy-metal pollution through wastewater are of interest to many researchers [1]. Over the past decades, this issue has been exacerbated by its association with the rapid growth in industrialization processes, so heavy-metal pollution in wastewater, especially from industrial waste, has become a major concern in terms of water pollution [1,2]. The sources of discharge of polluting heavy metals into natural water reservoirs come from various industries, including mining, smelting, refining of ores, fertilizer industries, manufacturing of electrical panels, tanneries, batteries, and paper industries [3,4]. These heavy metals are usually highly soluble in water, toxic, carcinogenic, and harmful to humans and aquatic life [5].

The release of these metals into the environment through various human and industrial activities is very harmful to the ecosystem because these pollutants are non-degradable, unlike organic pollutants, and can be transmitted through the food chain, causing their accumulation to lead to many diseases [6,7]. Due to the global water shortage, the search for strategies to ensure water security and sustainable use has become an urgent problem

* Corresponding author.
E-mail address: drsalahchem@uodiyala.edu.iq
DOI: 10.24237/djes.2025.18306

for which solutions are being sought continuously [8].

The well-known conventional methods, such as chemical precipitation, ion exchange, reverse osmosis, and organic solvent extraction, are the most widely used methods for removing heavy metals from wastewater [9]. Among all the processes used in water treatment, adsorption is a method with high removal efficiency and does not produce any harmful byproducts [10]. Adsorption is an attractive method for water purification, especially when the adsorbent is inexpensive and does not require pre-treatment before the adsorption process.

The use of specific microorganisms that have the ability to decompose pollutants or reduce their concentrations to an acceptable level, whether dead or alive, is known as biosorption; it is a convenient technique because it is inexpensive and very effective in removing pollutants [11]. Extensive research has focused on the utilization of biomass or its residues due to their abundant availability all over the world. In this perspective, biochar (BC), a solid carbon-rich byproduct produced by the pyrolysis of biomass, with the complete exclusion of oxygen at temperatures below 700 °C, is available from a wide range of low-cost biomass sources, including manure, organic waste, bioenergy crops (e.g., grasses and willows), and agricultural crop residues [12-15].

The intrinsic properties of BC, such as (a) high porosity, (b) high surface area, (c) large pore size, (c) availability of various functional groups, and (d) environmental friendliness, make it a potential candidate for wastewater treatment. Despite these properties, BC separation from aqueous solution is difficult due to its small particle sizes [16]. The separation of these particles from aqueous solutions requires a laborious process, such as filtration and centrifugation, thus limiting its practical application in wastewater treatment. Recent research has focused on the preparation of bound BC materials by immobilizing them within a semi-polymer containing sodium alginate with polyvinyl acetate [17–19]. Thermogravimetric analysis (TGA) assesses the thermal stability and decomposition of algae-derived char by tracking weight loss during heating, moisture, organic degradation, and ash content. Brunauer–Emmett–Teller (BET) analysis measures surface area, porosity, and pore size distribution. These techniques are essential for characterizing BC, catalysts, and sorbents and linking material properties to performance. TGA helps optimize pyrolysis conditions, and BET assesses sorption capacity. Both analyses provide essential insights for developing sustainable materials [20,21]. The present work specifically examined the adsorption performance of BC derived from Chara algae for the removal of lead and copper ions from aqueous solutions. Key parameters, including pH, contact time, adsorbent dosage, and initial metal concentration, were systematically evaluated to improve adsorption efficiency. Advanced kinetic modelling and FTIR, scanning electron microscopy (SEM), and energy-dispersive X-ray spectroscopy (EDS) investigations were performed to reveal the underlying adsorption mechanisms, and reusability studies were conducted to evaluate the practical limitations and advantages of the adsorbent. This study aims to provide an in-depth understanding of heavy metal ion adsorption mechanisms and identify operating conditions through an integrated scientific approach that combines experimental research and advanced sorbent characterization. This approach contributes to the development of effective and sustainable solutions for treating contaminated water.

## 2. Materials and Methods

### *2.1. Preparation of BC From Chara Algae*

The algae (C. vulgaris) used in this study were collected in October from Khorasan River in Baqubah, Iraq. They were washed with normal water several times and then with distilled water to remove the suspended dirt. They were dried under the sun for 2 days and then placed in an oven at 75 °C for a whole day to complete the drying process. The dried algae were ground and isolated using molecular sieves to obtain 300–600 μm of dried algae and then stored in a plastic bottle. Burning and calcining were carried out in isolation from air in a steel tube at

temperatures between 400 °C and 600 °C. Afterwards, the samples were cooled and stored in plastic tubes for use in experiments.

*2.2 Metal Solutions*

Chemicals from well-known international companies DIFCO, Sigma, Mallinckrot, and Fisher were used. Within analytical grade whenever available, 1 L of standard solutions of copper and lead ions was prepared by dissolving specified amounts of lead nitrate and copper chloride in water. The water was distilled several times and passed over specific resins to remove any ions to ensure that precipitation did not occur. A solution of different concentration was prepared from the prepared standard solution. The pH was controlled by adding drops of 0.1 N $HNO_3$ or NaOH.

*2.3. Characterization of BC*

*2.3.1 TGA and BET Analysis*

TGA was performed using an automated model in a nitrogen atmosphere (flow rate of 50 ml/min) with a heating rate of 10 °C/min from 30 °C to 800 °C to evaluate the thermal decomposition at the Water Research Center of the Ministry of Science and Technology by using a Perkin-Elmer 4000 top-loading thermogravimetric analyzer. The BET technique was performed using a US-based thermogravimetric analyzer at the Petroleum Research and Development Center of the Iraqi Ministry of Oil.

*2.3.2 FTIR Analysis*

FTIR analysis was performed using Perkin-Elmer Spectrum 100 to identify functional groups on the BC surface before and after copper and lead adsorption. Spectra were recorded at the wavelength of 4000–400 $cm^{-1}$ to determine the presence of functional groups, such as hydroxyl, carbonyl, and carboxyl, which play an important role in the process of absorption of lead and copper ions [22–24].

*2.3.3. SEM Analysis*

The surface morphology of BC before and after adsorption of metal ions was studied using SEM (Axia ChemiSEM scanning electron microscope). Samples were coated with a thin layer of gold by using a spray layer to improve conductivity. Images were taken at magnifications ranging from 5× to 1,000,000× to visualize surface texture and pore structure [25–27].

*2.3.4. EDS Analysis*

The elemental composition of the BC surface before and after adsorption was analyzed using EDS coupled with SEM. Spectra were acquired at an accelerating voltage of 30 kV to determine the presence of copper and lead ions adsorbed on the BC surface [26].

*2.4 Metal Uptake*

The amount of absorbed material q was calculated using the following equation [27]:

$$q = \frac{V * (C_o - C_e)}{m * 1000} \qquad (1)$$

where q represents amount of metal adsorbed on algae in (mg/g); $C_0$ and $C_e$ represent the concentration at time zero and the final concentration (equilibrium concentration) of ions in mg/L, respectively; V is the mixture volume in mL; and m is the weight of the algae used in g.

*2.5 Isotherm Study*

Equilibrium data were analyzed using Langmuir and Freundlich equation models to determine the adsorption behavior and maximum adsorption capacity.

Langmuir model:

$$\frac{C_e}{q_e} = \frac{1}{q_m K_L} + \frac{C_e}{q_m} \qquad (2)$$

Freundlich model:

$$\ln q_e = \ln qK_F + \frac{1}{n} \ln C_e \qquad (3)$$

## 3. Results and Discussion

*3.1 Characterization Analysis*

*3.1.1 TGA and BET Analysis*

Initially from 25 °C to 150 °C, a slight drop in weight can be observed at temperatures between 25 °C and 150 °C due to weight loss associated with surface moisture; between 150 °C and 400 °C, the surface groups disintegrated; and at 400 °C–700 °C, the aromatic carbon structure

decomposed (Figure 1 for TGA). After 700 °C, the weight stabilized, and only ash and minerals remained. The BET analysis of BC produced from algal biomass via semi-anaerobic pyrolysis at 500 °C showed a BET surface area of 250 $m^2/g$, with a total pore volume of 0.3 $cm^3/g$, dominated by mesopores (20 nm). This moderate surface area arose from the unique composition of algae, containing proteins and carbohydrates that decompose into volatile compounds, leaving behind a porous carbon structure. The porosity is lower than that of cellulosic materials due to the presence of inorganic minerals such as calcium and magnesium.

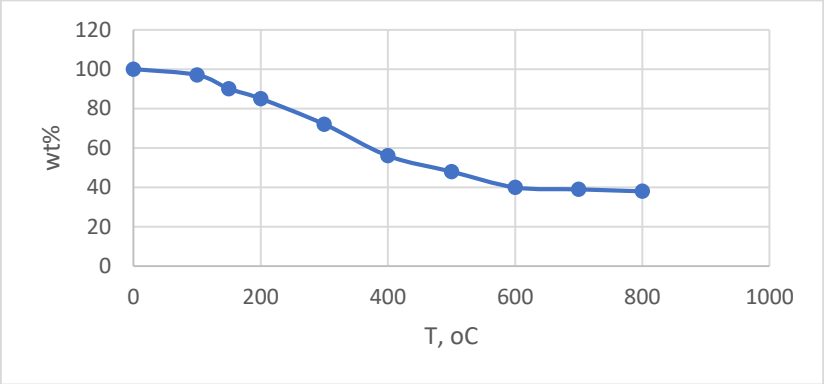


**Figure 1.** Thermogravimetric analysis of biochar

*3.1.2 FTIR Analysis*

Figure 2 shows the FTIR spectra for algae and calcinated algae at 400 °C, 500 °C, and 600 °C. Comparison of the FTIR spectrum of algae before and after calcination at 600 °C showed that both spectra shared a similar trend, indicating the continued presence of some functional groups after calcination. However, the main differences are clear as follows:

- The expansion band of the OH group near 3500 $cm^{-1}$ decreased slightly in the calcined sample, indicating dehydration and loss of hydroxyl groups.
- In the region of 1500–500 $cm^{-1}$, the shifts and peak intensity changes reflected the structural changes in the organic matrix.
- The calcined sample showed weakened peaks in regions associated with organic functional groups (e.g., CH and C=O), indicating significant decomposition of organic materials during calcination.
- The remaining material is likely composed of inorganic compounds (such as CaO, MgO, or mineral phases) formed after organic removal.

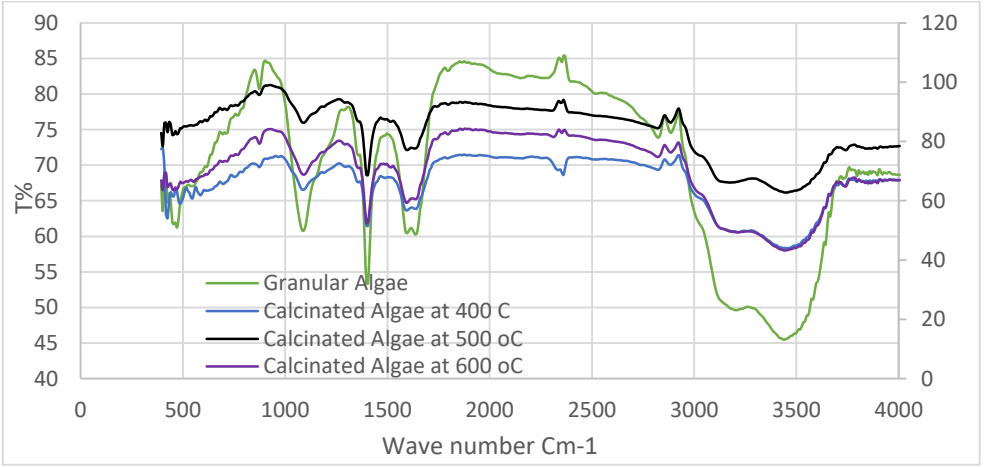


**Figure 2.** FTIR spectrum for algae and calcinated algae at 400,500,and 600 ºC

Figures 3–6 show the behavior of algae after adsorption with copper and lead ions. The spectrum shows a comparison between algae calcined at 600 °C and the same algae after adsorption of lead ions. The clear differences in the spectrum reflected the chemical changes that occurred on the surface of the material because of its interaction with lead, providing direct evidence of the adsorption mechanism. A clear decrease in transmittance ratio can be observed across the spectrum after lead adsorption, indicating changes in the chemical composition of the solid. Such decrease exhibited that the lead molecules reacted with the functional groups on the surface of the calcined algae, forming new bonds or modifying the original chemical structure. Changes occurred in the functional groups responsible for adsorption. The absorption band at 3500 $cm^{-1}$ (O–H) showed a noticeable change in the intensity and position of the broad band associated with the hydroxyl group (–OH). This change reflects hydroxylation in the process of binding to lead ions, whether through hydrogen bonds or direct interaction with them.

The change occurring within the range of 1600–1400 $cm^{-1}$ (C=O or C=C) indicated that the carbon double bonds available in the carboxyl groups contributed to the absorption of lead ions through complexation or ion exchange. In the region between 1000 and 500 $cm^{-1}$, a noticeable shift occurred in the peaks, which is related to the formation of new bonds between lead ions and the remaining metallic elements in the calcined algae, such as the reaction of Pb with Si–O, Al–O, or Ca–O. These spectral changes likely demonstrated that lead was associated with calcined algae through forming bonds with hydroxyl and carboxyl groups, interaction with the remaining mineral components after calcination, and physical adsorption or ion exchange, as revealed by changes in the fingerprint area.

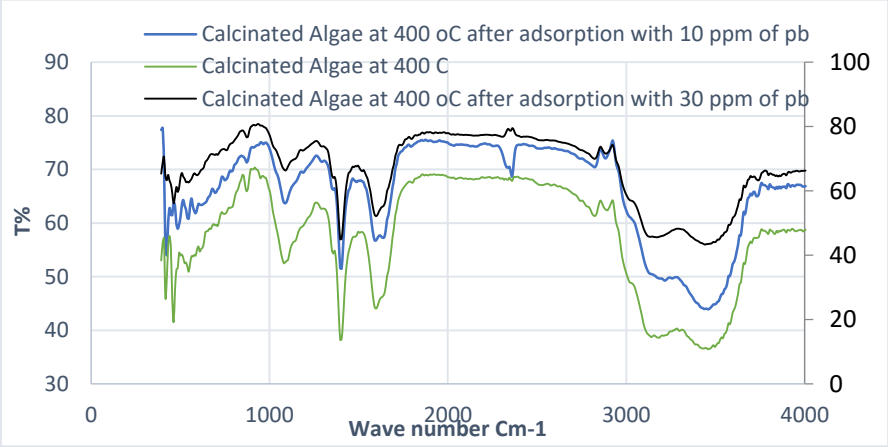


**Figure 3.** FTIR spectrum for calcinated algae at 400 ºC befor and after adsorption with 10,30 ppm of lead

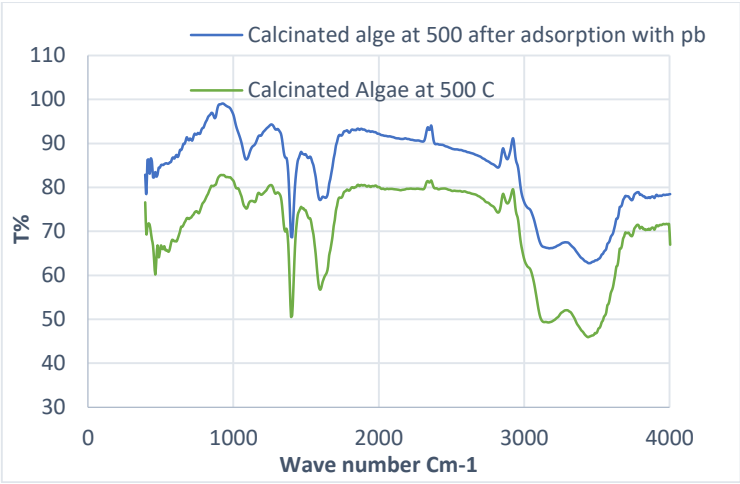


**Figure 4.** FTIR spectrum for calcinated algae at 500 ºC befor and after adsorption with 10 ppm of lead

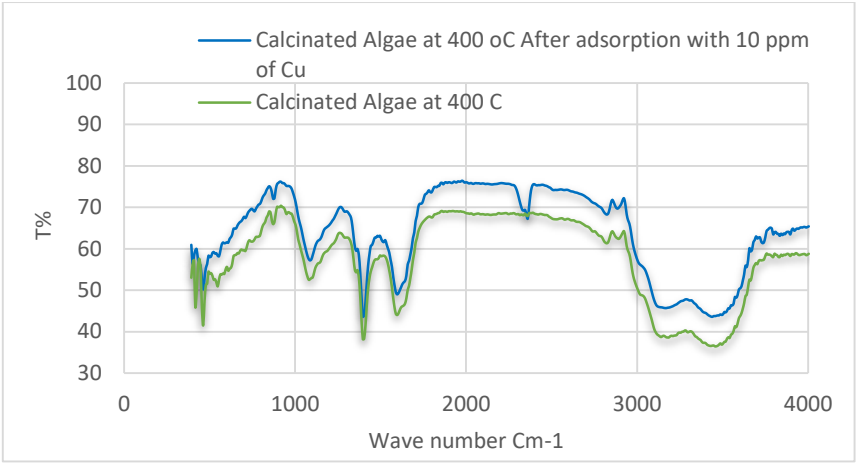


**Figure 5.** FTIR spectrum for calcinated algae at 400 ºC befor and after adsorption with 10 ppm of copper

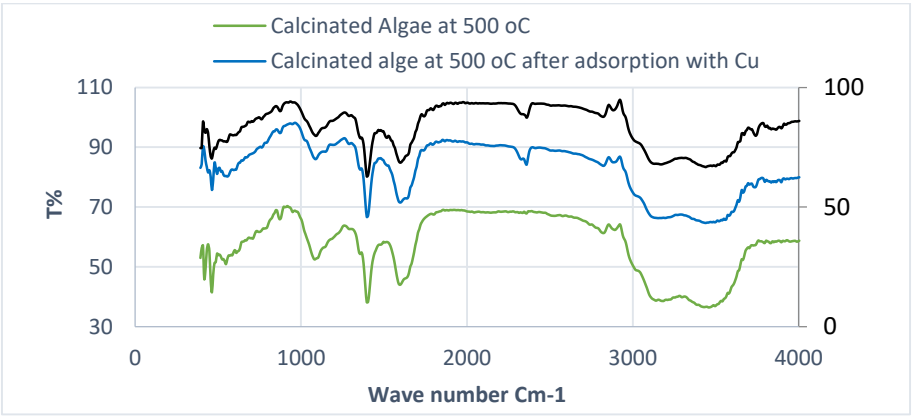


**Figure 6.** FTIR spectrum for calcinated algae at 500 ºC befor and after adsorption with 10,30 ppm of copper

### *3.1.3 SEM and EDS Analysis*

#### *3.1.3.1. SEM*

Figures 7 and 8 show that the BC structure from 400 micron to 500 nm clearly showed highly porous structures. Figure 9 shows the structure after the adsorption of lead ions, and Figure 10 shows the structure after the adsorption of copper ions. After adsorption, the BC surface appeared to be smoother with visible particle agglomeration, indicating metal ion deposition.

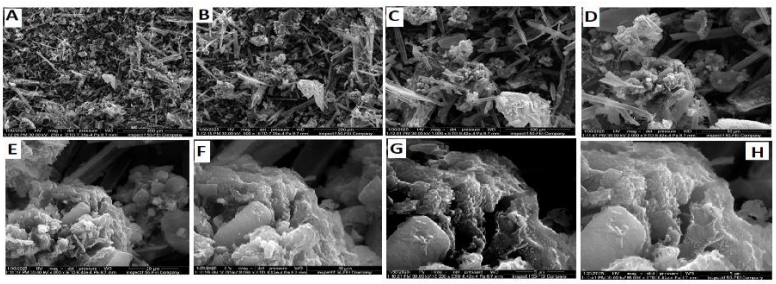


**Figure 7.** SEM image of raw biochar (A 400 B 200, C 100 , D 50, E 20 , F 10 ,and both Gand H are 5 micron)

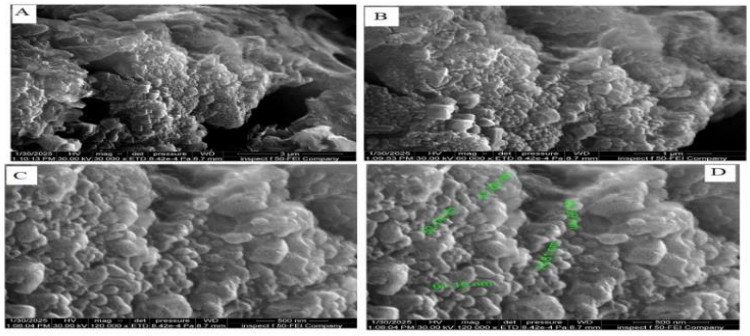


**Figure 8.** SEM image of raw biochar from A 3 micron to D 500 nanometre

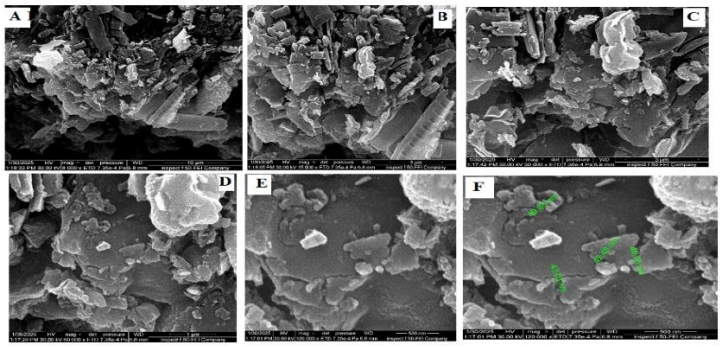


**Figure 9.** Structures after adsorption of lead ions A 10, B 5, C 3, D 1 micron, E and F are 500 nanometres

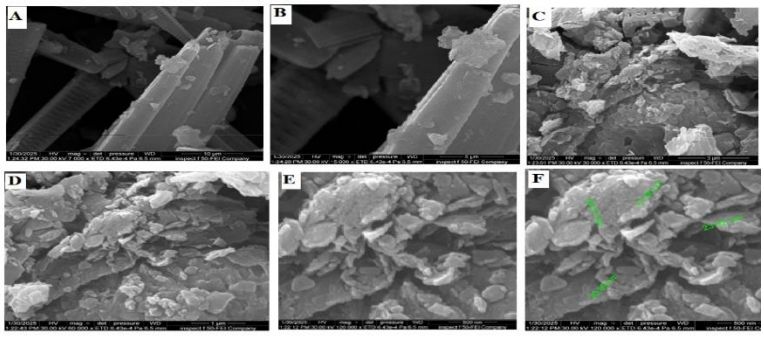


**Figure 10.** Structures after adsorption of copper ions

*3.1.3.2 EDS*

EDS (Figure 11) confirmed the presence of copper and lead peaks post-adsorption, verifying successful metal uptake by BC. Before adsorption, major elements like C, O, and H dominated BC. After adsorption, new peaks for copper and lead were found, confirming adsorption. The displacement of $Ca^{2+}$ and $Mg^{2+}$ from BC suggests ion exchange as a key mechanism. The presence of oxygen-containing functional groups (–COOH and –OH) promoted metal binding through complexation. At low pH levels, $Pb^{2+}$ and $Cu^{2+}$ bind to negatively charged BC sites via electrostatic interaction. The precipitation suggested by the EDS results demonstrated evidence for potential metal hydroxide precipitation, further aiding removal efficiency. Table 1 provides an elemental composition before adsorption.

**Table 1** Average EDS composition (weight%) for bio char before adsorption

| Element | Atomic % | Atomic % Error | Weight % | Weight % Error |
|---|---|---|---|---|
| C | 26.5 | 0.2 | 17.7 | 0.1 |
| O | 56.1 | 0.3 | 49.9 | 0.3 |
| Mg | 0.7 | 0.0 | 0.9 | 0.0 |
| Al | 0.6 | 0.0 | 1.0 | 0.0 |
| Si | 8.0 | 0.0 | 12.5 | 0.1 |
| K | 0.5 | 0.0 | 1.0 | 0.0 |
| Ca | 7.6 | 0.0 | 17.0 | 0.1 |

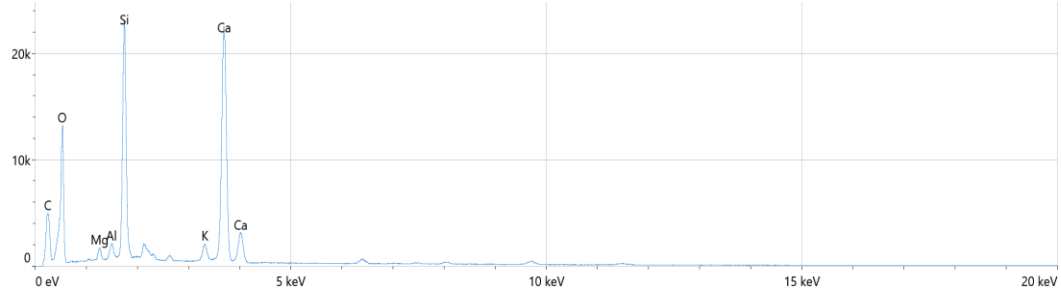


**Figure 11.** EDS spectrum with labeled peaks and inset elemental maps for biochar.

Figure 12 shows the EDS results after adsorption of lead ions, Table 2 shows the elemental composition after lead adsorption, and Figure 13 shows the EDS results after adsorption with lead and copper ions. The spectra showed prominent peaks for carbon (C) and hydrogen (O), which are indicative of the organic matrix of the charcoal and oxygen-containing functional groups (e.g., carboxyl and hydroxyl), attributed to the association of minerals via complexes and ion exchange. Calcium and other trace minerals (e.g., $Ca^{2+}$ and $Mg^{2+}$) participate in the yellow ion-exchange sites to segregate the metal. The post-adsorption EDS results showed peaks for lead or copper starting at low concentrations, clearly indicating effective light concentrations. The absence of toxic products or significant leaching indicated bright light indicators, enhancing suitability for aquatic applications. These results included FTIR and SEM data, which collectively illustrate the causes of many functional problems.

**Table 2.** Average EDS composition (weight%) for bio char After lead adsorption

| Element | Atomic % | Atomic % Error | Weight % | Weight % Error |
|---|---|---|---|---|
| C | 36.2 | 0.5 | 25.4 | 0.4 |
| O | 48.0 | 0.6 | 44.8 | 0.5 |
| Mg | 0.7 | 0.0 | 1.0 | 0.1 |
| Al | 0.6 | 0.0 | 1.0 | 0.0 |
| Si | 9.4 | 0.1 | 15.4 | 0.1 |
| K | 0.3 | 0.0 | 0.6 | 0.1 |
| Ca | 4.7 | 0.0 | 10.9 | 0.1 |
| Ni | 0.1 | 0.0 | 0.5 | 0.1 |
| Pb | 0.0 | 0.0 | 0.3 | 0.2 |

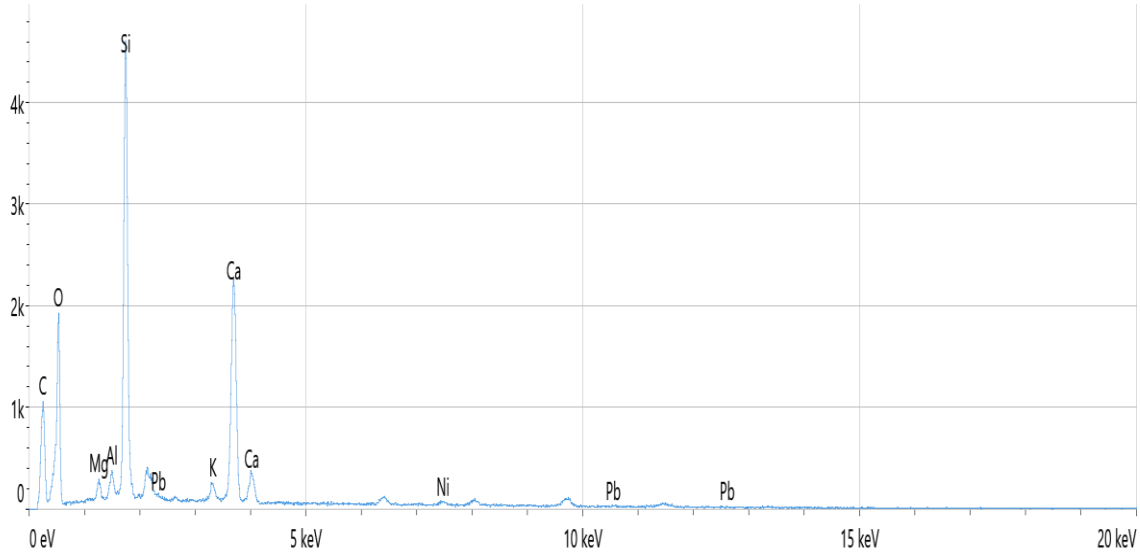


**Figure 13.** EDS spectrum with labeled peaks and inset elemental maps after lead adsorption.

Figure 14 shows the EDS results after adsorption of copper ions, Table 3 shows the elemental composition after copper adsorption, and Figure 23 shows the EDS results after adsorption with lead and cooper ions.

**Table 3.** Average EDS composition (weight%) for bio char After copper adsorption

| Element | Atomic % | Atomic % Error | Weight % | Weight % Error |
|---|---|---|---|---|
| C | 26.7 | 0.2 | 17.7 | 0.2 |
| O | 55.6 | 0.3 | 49.1 | 0.3 |
| Mg | 0.7 | 0.0 | 0.9 | 0.0 |
| Al | 0.6 | 0.0 | 0.9 | 0.0 |
| Si | 8.0 | 0.0 | 12.5 | 0.1 |
| K | 0.5 | 0.0 | 1.0 | 0.0 |
| Ca | 7.6 | 0.0 | 16.7 | 0.1 |
| Fe | 0.2 | 0.0 | 0.6 | 0.0 |
| Cu | 0.1 | 0.0 | 0.4 | 0.0 |

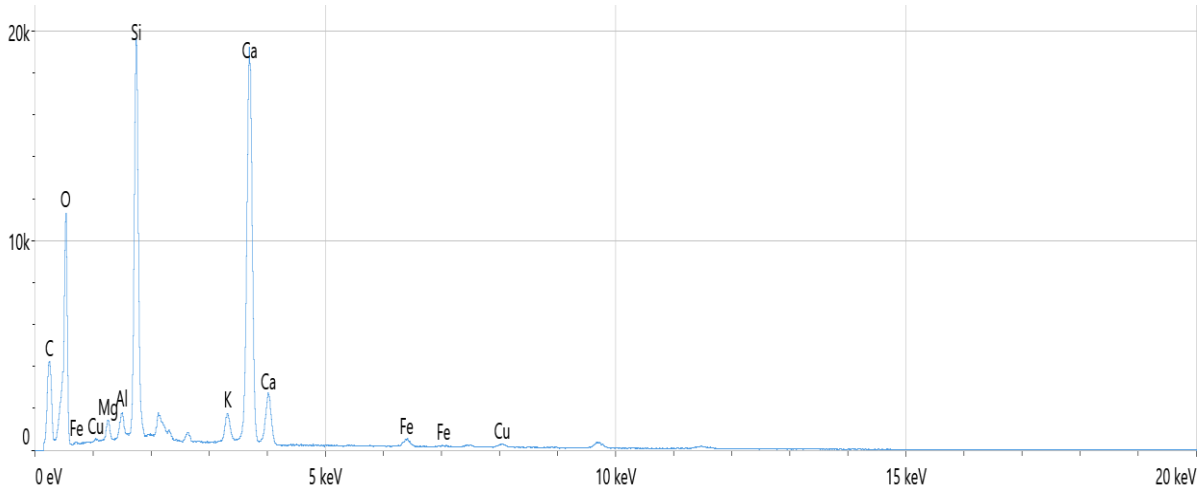


**Figure 14.** EDS spectrum with labelled peaks and inset elemental maps after copper adsorption.

The FTIR results demonstrated that the shift of the –OH expansion band from 3420 $cm^{-1}$ to 3380 $cm^{-1}$ after the adsorption of copper and lead indicated the interaction between hydroxyl groups and metal ions. The carboxyl peak (C=O) at 1720 $cm^{-1}$ changed, indicating complexation with metal ions. These spectral changes are supported by the EDS results, as seen in the tables of elemental composition before and after adsorption. As shown in Table 4, BC achieved concentrations of 322 mg/g for lead and 196 mg/g for copper, surpassing rice charcoal under the same conditions and manganese oxide-activated charcoal. This improvement is attributed to its high porosity and functional groups [22,27,29].

**Table 4.** Comparison meta up take

| reference | pH | T | Biochar Type | q mg/g | Our biochar |
|---|---|---|---|---|---|
| Sun et al. (2019) | 5 | 25 | Rice husk | 148 pb | 322 |
| Liu et al. (2020) | 5 | 35 | Rice husk | 45 cu | 196 |
| Tan et al. (2015) | 6 | 25 | MnO2-biochar | 153 pb | 322 |
| Chen et al. (2015) | 5 | 25 | Chitosan-modified | 105 cu | 196 |

*3.2 Effect of pH*

Figures 15 and 16 show that adsorption did not occur at low pH levels due to the competition of protons with metals for the active sites responsible for biosorption, which reduced the adsorption of the metal. The pH of the solution is an important parameter to control the adsorption process. Therefore, the effect of pH on the adsorption process of lead and copper ions was examined. Figure 15 shows that the adsorption process increased steadily with increasing pH, reached its maximum at pH 6, and then started decreasing after 6–8 due to the medium turning into an alkaline medium. The decrease in the adsorption process at low levels of the acidity scale is due to the competition between heavy metal ions and the $H_3O$ ion for the active sites in BC [19–22,29–30]. Therefore, at a low pH level, an increase in protons occurred, which competed with heavy-metal ions for active sites, resulting in reduced or even no adsorption process. Other researchers obtained the same results [23–25].

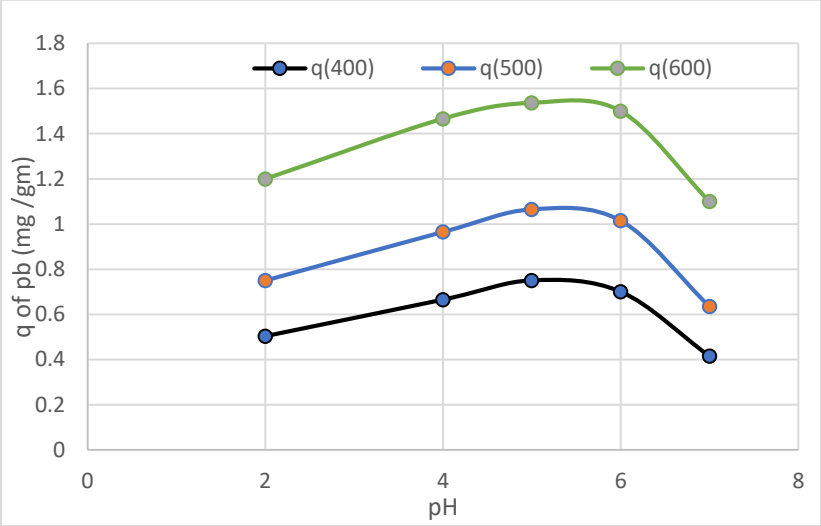


**Figure 15**. Lead uptake(q) with pH at different calcination temperatures.

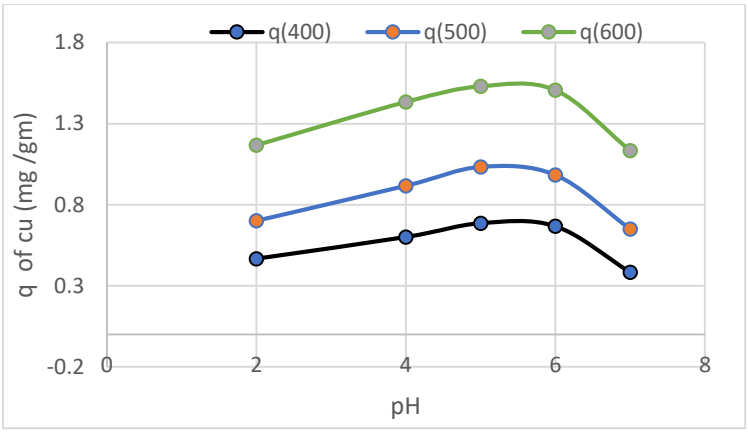


**Figure 16.** Copper uptake(q) with pH at different calcination temperatures.

*3.3 Effect of Temperature*

Figure 17 shows the effect of temperature on the adsorption capacity (q, mg/g) of the adsorbent for lead and copper ions. The adsorption capacity for both metals increased with temperature, reaching a peak at about 45 °C (~75 mg/g for lead and ~50 mg/g for copper), followed by a slight decrease at higher temperatures. This trend indicated that the adsorption process is endothermic, which occurs in chemical adsorption as opposed to physical adsorption, which is exothermic. High temperatures enhance the mobility of metal ions and their interaction with active sites on the adsorbent. The subsequent decrease in adsorption after 50 °C can be attributed to the adsorption effects or structural changes in the adsorbent at increased temperatures [30,31].

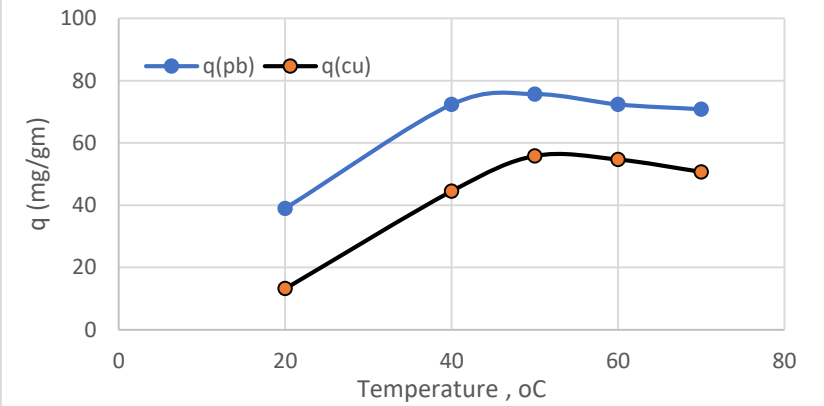


**Figure 17.** Lead and copper sorption capacity with temperature

*3.4 Effect of Different Initial Metal Concentrations*

As shown in Figures 18–20, the biosorption increased with increasing initial concentration due to the availability of binding sites for ions because the higher initial concentration of heavy metal ions increased the probability of collision with adsorption sites on the surface of the adsorbent. In addition, the driving force for mass transfer is better, which helps reduce the mass transfer resistance and increases the adsorption capacity [30]. As shown in Figure 20, the biosorption process was rapid in the first 15 min, and then the concentration decreased during the remaining period. The concentrations of metals in the liquid continued to decrease and

reached the equilibrium value. The first faster phase of biosorption of metals is attributed to surface adsorption due to the ion exchange action with the participation of some functional groups, and the second lower phase may represent the diffusion of metal ions into the sites within BC.

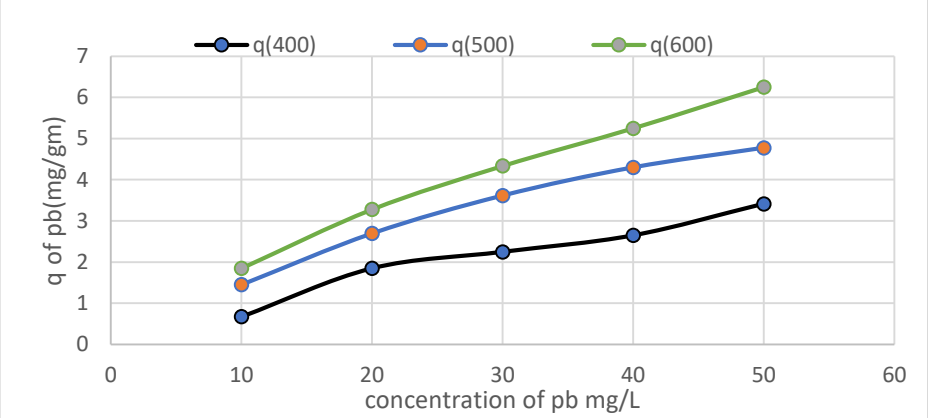


**Figure 18.** Adsorption capacity of lead at different initial concentration

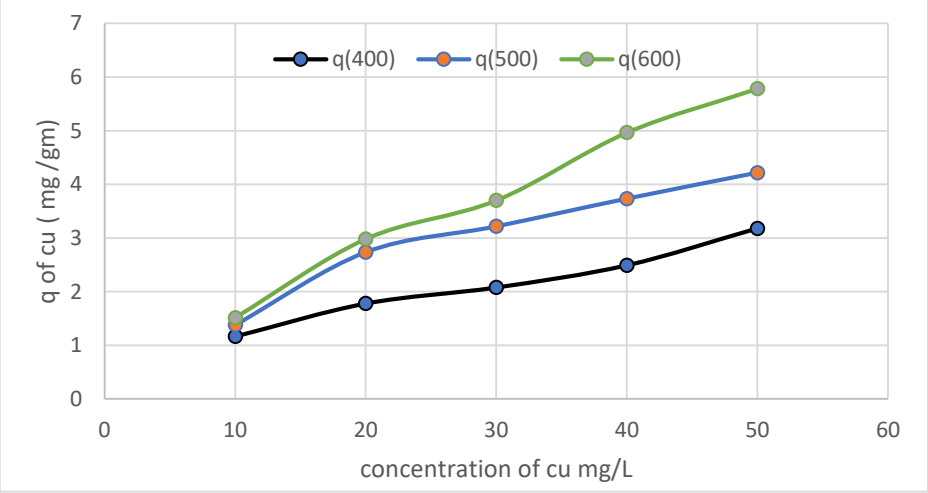


**Figure 19** Adsorption capacity of copper at different initial concentration

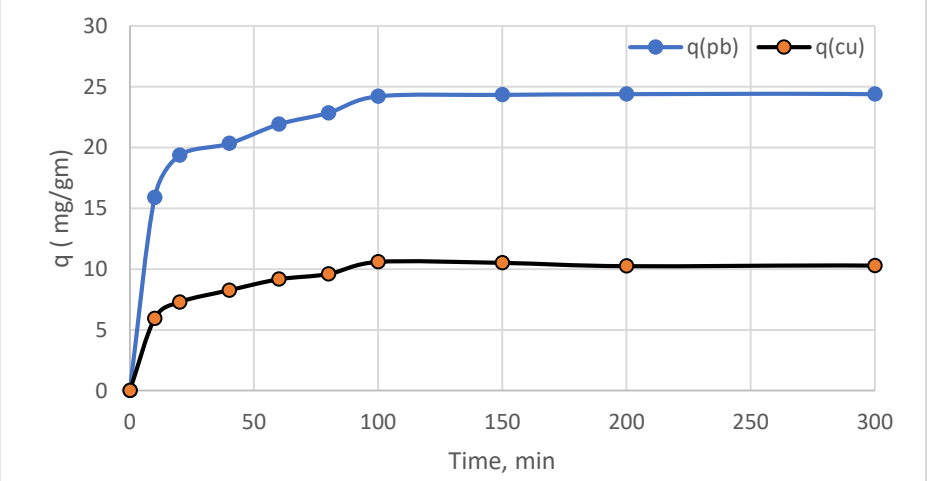


**Figure 20** Metal uptake with time at different initial concentrations.

*3.5 Effect of Adsorbent Dose*

The dosage of the adsorbent was studied, as shown in Figure 21. With the increase in the amount of adsorbent, the removal rates of lead and copper increased. As the amount of BC increased, the metal uptake decreased due to the interaction of binding sites [32].

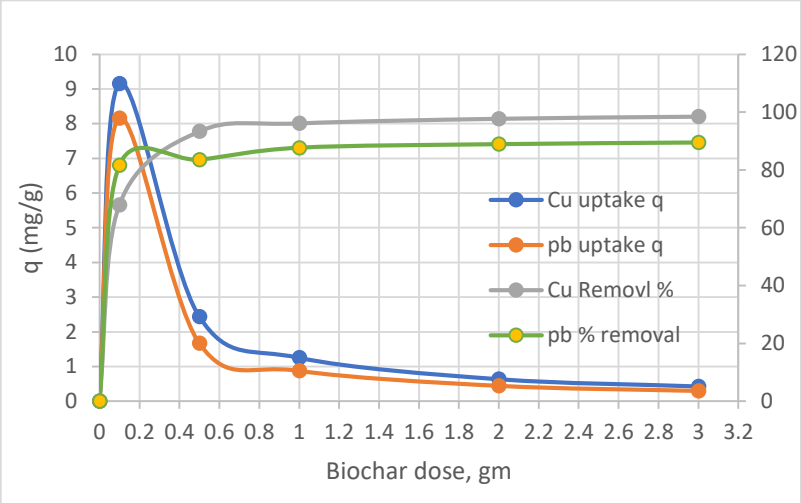


**Figure 21.** Relationship between adsorbent dose, concentration gradients and q

*3.6 Isotherm Results*

Figures 22–25 show the Langmuir and Freundlich isotherms on the experimental data. The suitability of each model was assessed on the basis of correlation coefficient ($R^2$) and the closeness of experimental and calculated values. Table 5 summarizes the fit data with each model, implying the adsorption mechanism (monolayer vs. multilayer and homogeneous vs. heterogeneous). Both models provided good agreement with the data, suggesting that the adsorption process may involve single- and multilayer adsorption mechanisms, possibly due to surface heterogeneity or a combination of physical and chemical adsorption.

**Table 5.** Adsorption Isotherms

| Pollutant | Langmuir | | | Freundlich | | |
|---|---|---|---|---|---|---|
| parameter | qm (mg/g) | KL(L/mg) | $R^2$ | nmg/g | kf | $R^2$ |
| Pb | 322 | 0.037 | 0.98 | 1.5 | 15.00 | 0.963 |
| Cu | 196 | 0.070 | 0.98 | 1.715 | 16.78 | 0.987 |

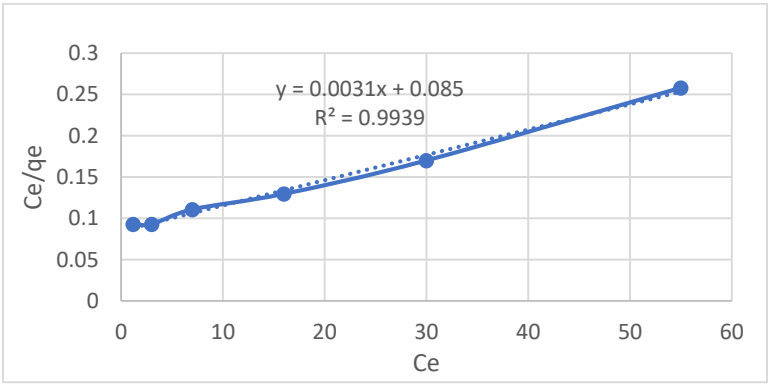


**Figure 22.** Copper Langmuir model

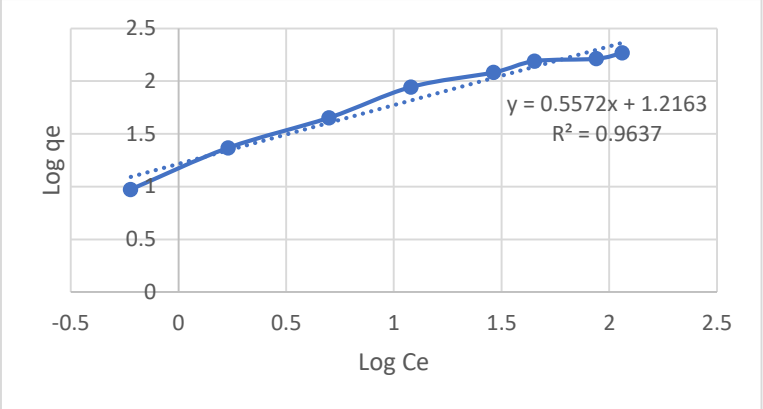


**Figure 23**. Copper Freundlich model

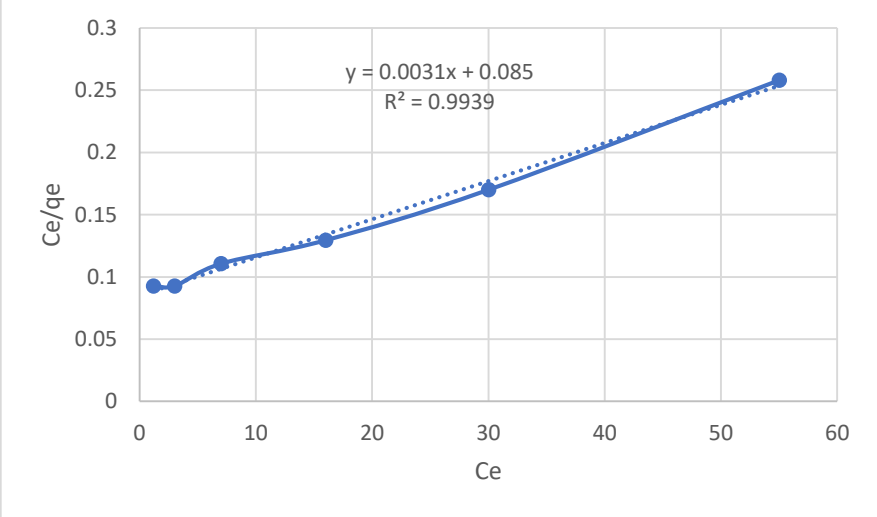


**Figure 24.** Lead Langmuir model

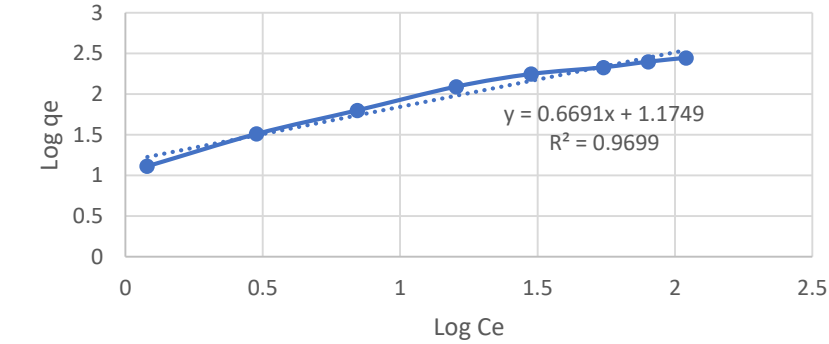


**Figure 25.** Lead Freundlich model

The adsorption equilibrium data were best fitted by the Langmuir isotherm model ($R^2$ > 0.98), suggesting monolayer adsorption on a homogeneous surface. The maximum adsorption capacity of lead was higher at 322 mg/g than that of copper at 196 mg/g.

## 4. Conclusions

This study highlights the potential of biochar (BC), derssived from Chara algae, as a highly efficient and sustainable adsorbent for the removal of heavy metals from aqueous solutions. Under best conditions (pH 5-6, sorbent dosage 1.0 g/L), the biochar exhibited high adsorption efficiencies of 322 mg/g for $Pb^{2+}$ and 196 mg/g for $Cu^{2+}$. Advanced material

characterization using Fourier transform infrared spectroscopy (FTIR) and scanning electron microscopy (SEM-EDS) analysis attributed this performance to the sophisticated porous structure of the biochar and the abundance of active functional groups present on its surface.

## References


[1] H. A. Alalwan, M. A. Kadhom, and A. H. Alminshid, "Removal of heavy metals from wastewater using agricultural byproducts," *J. Water Supply Res. Technol. - Aqua*, vol. 69, no. 2, pp. 99–112, Mar. 2020. **DOI:** 10.2166/aqua.2020.133

[2] M. Thakare et al., "Understanding the holistic approach to plant-microbe remediation technologies for removing heavy metals and radionuclides from soil," *Curr. Res. Biotechnol.*, vol. 3, pp. 84–98, 2021. **DOI:** 10.1016/j.crbiot.2021.02.004

[3] S. K. Gunatilake, "Methods of removing heavy metals from industrial wastewater," *J. Multidiscip. Eng. Sci. Stud.*, vol. 1, no. 1, pp. 12–18, Nov. 2015.

[4] H. Sarma and M. N. V. Prasad, "Phytomanagement of polycyclic aromatic hydrocarbons and heavy metals-contaminated sites in Assam, north eastern state of India, for boosting bioeconomy," in *Bioremediation and Bioeconomy*, Elsevier, 2016, pp. 609–626. **DOI:** 10.1016/B978-0-12-802830-8.00024-1

[5] N. R. Lynch, T. C. Hoang, and T. E. O'Brien, "Acute toxicity of binary-metal mixtures of copper, zinc, and nickel to *Pimephales promelas*: Evidence of more-than-additive effect," *Environ. Toxicol. Chem.*, vol. 35, no. 2, pp. 446–457, Feb. 2016. **DOI:** 10.1002/etc.3204

[6] M. Bilal et al., "Waste biomass adsorbents for copper removal from industrial wastewater—A review," *J. Hazard. Mater.*, vol. 263, pp. 322–333, Dec. 2013. **DOI:** 10.1016/j.jhazmat.2013.07.071

[7] I. Noor et al., "Heavy metal and metalloid toxicity in horticultural plants: Tolerance mechanism and remediation strategies," *Chemosphere*, vol. 302, p. 135196, 2022. **DOI:** 10.1016/j.chemosphere.2022.135196

[8] X. Liu et al., "Membrane technology for rainwater treatment and reuse: A mini review," *Water Cycle*, vol. 2, pp. 51–63, 2021. **DOI:** 10.1016/j.watcyc.2021.08.001

[9] N. Ahalya, T. V. Ramachandra, and R. D. Kanamadi, "Biosorption of heavy metals," *Res. J. Chem. Environ.*, vol. 7, no. 4, pp. 71–79, 2003.

[10] P. N. Diagboya, B. I. Olu-Owolabi, F. M. Mtunzi, and K. O. Adebowale, "Clay-carbonaceous material composites: Towards a new class of functional adsorbents for water treatment," *Surf. Interfaces*, vol. 19, p. 100506, 2020. **DOI:** 10.1016/j.surfin.2020.100506

[11] S. N. Farhan, W. A. Mahmood, M. H. Ismael, A. A. Khadom, and A. M. A. Karim, "Biosorption of copper and lead ions using *Chara* algae," *Pak. J. Eng. Appl. Sci.*, vol. 29, pp. 1–6, Jul. 2021.

[12] M. U. Mustapha et al., "Microorganisms and biosorption of heavy metals in the environment: A review paper," *J. Microb. Biochem. Technol.*, vol. 7, no. 5, pp. 253–256, 2015. **DOI:** 10.4172/1948-5948.1000219

[13] S. N. Farhan and A. A. Khadom, "Biosorption of heavy metals from aqueous solutions by *Saccharomyces cerevisiae*," *Int. J. Ind. Chem.*, vol. 6, pp. 119–130, 2015. **DOI:** 10.1007/s40090-015-0038-8

[14] J. Lehmann and S. Joseph, Eds., *Biochar for Environmental Management: Science, Technology and Implementation*, 2nd ed. Routledge, 2015. **DOI:** 10.4324/9780203762264

[15] J. Lehmann et al., "Biochar effects on soil biota—A review," *Soil Biol. Biochem.*, vol. 43, no. 9, pp. 1812–1836, 2011. **DOI:** 10.1016/j.soilbio.2011.04.022

[16] Y. Ding et al., "Evaluation of biochar effects on nitrogen retention and leaching in multi-layered soil columns," *Water Air Soil Pollut.*, vol. 213, pp. 47–55, 2010. **DOI:** 10.1007/s11270-010-0366-4

[17] W. Kwapinski et al., "Biochar from biomass and waste," *Waste Biomass Valor.*, vol. 1, pp. 177–189, 2010. **DOI:** 10.1007/s12649-010-9024-8

[18] D. Mohan, A. Sarswat, Y. S. Ok, and C. U. Pittman, Jr., "Organic and inorganic contaminants removal from water with biochar, a renewable, low cost and sustainable adsorbent—A critical review," *Bioresour. Technol.*, vol. 160, pp. 191–202, 2014. **DOI:** 10.1016/j.biortech.2014.01.120

[19] R. Wang et al., "Effects of chlortetracycline and copper on tetracyclines and copper resistance genes and microbial community during swine manure anaerobic digestion," *Bioresour. Technol.*, vol. 238, pp. 57–69, 2017. **DOI:** 10.1016/j.biortech.2017.03.134

[20] Neto, Jorge SS, et al. "A review on the thermal characterisation of natural and hybrid fiber composites." Polymers 13.24 (2021): 4425. DOI:10.3390/polym13244425

[21] D. Losic, F. Farivar, P. L. Yap, and A. Karami, "Accounting carbonaceous counterfeits in graphene materials using the thermogravimetric analysis (TGA) approach," *Analytical Chemistry*, vol. 93, no. 34, pp. 11859-11867, 2021.

[22] B. Cu and A. Zn, "Biosorption of Cu2+ and Zn2+ by immobilized algae biomass of chlorella kessleri," Acta Metallurgica Slovaca, vol. 15, no. 4, pp. 255-263, 2009.

[23] A. Stoll and J. R. Duncan, "Comparison of the heavy metal sorptive properties of three types of immobilized, non-viable *Saccharomyces cerevisiae* biomass," *Process Biochem.*, vol. 32, no. 6, pp. 467–472, 1997. **DOI:** 10.1016/S0032-9592(96)00093-3

[24] S. Shindo and M. Kamimura, "Immobilization of yeast with hollow PVA gel beads," *J. Ferment. Bioeng.*, vol. 70, no. 4, pp. 232–234, 1990. **DOI:** 10.1016/0922-338X(90)90054-Z

[25] T. Wei et al., "Performance of heavy metal-immobilizing bacteria combined with biochar on remediation of cadmium and lead co-contaminated soil," *Environ. Geochem. Health*, vol. 45, pp. 6009–6026, 2023. **DOI:** 10.1007/s10653-023-01605-9

[26] M. Varnaseri-Ghandali et al., "Adsorption of multi-heavy metals from aqueous solution by wheat straw and its biochar loaded with $MnO_2$ nanoparticles: Characteristics and mechanisms," *Environ. Dev. Sustain.*, 2024. **DOI:** 10.1007/s10668-024-05238-5

[27] Tan, X. *et al.* (2015) 'Application of biochar for the removal of pollutants from aqueous solutions', *Chemosphere*, 125, pp. 70–85.

[28] X. Lin, J. Zhou, and S. Sun, "Cadmium and lead removal by Mg/Fe bimetallic oxide-loaded sludge-derived biochar: Batch adsorption, kinetics, and mechanism," *Environ. Sci. Pollut. Res.*, vol. 30, pp. 86866–86878, 2023. **DOI:** 10.1007/s11356-023-28574-x

[29] T. Liu et al., "Structural characteristics of biochars made from different parts of corn straw and their adsorption performances for methylene blue," *J. Water Process Eng.*, vol. 68, p. 106562, 2024. **DOI:** 10.1016/j.jwpe.2024.106562

[30] X. Shi et al., "The Application of Biochar as Heavy Metals Adsorbent: The Preparation, Mechanism, and Perspectives," *Int. J. Environ. Res.*, vol. 18, p. 41, 2024. **DOI:** 10.1007/s41742-024-00592-8

[31] S. Gu and C. Q. Lan, "Effects of culture pH on cell surface properties and biosorption of Pb(II), Cd(II), Zn(II) of green alga *Neochloris oleoabundans*," *Chem. Eng. J.*, vol. 468, p. 143722,2023. **DOI:** 10.1016/j.cej.2023.143579.

[32] J. Di et al., "Adsorption behaviors and mechanisms of Cu2+, Zn2+ and Pb2+ by magnetically modified lignite," Scientific Reports, vol. 12, no. 1, p. 1394, 2022. **DOI:** 10.1038/s41598-022-05453-y